Chem
Europ

European C
Societies P

Check for
updates

Crystalline Copper Selenide as a Reliable Non-Noble Electro(pre)catalyst for Overall Water Splitting

Biswarup Chakraborty+,[a] Rodrigo Beltrán-Suito+,[a] Viktor Hlukhyy,[b] Johannes Schmidt,[c] Prashanth W. Menezes,*[a] and Matthias Driess*[a]

Electrochemical water splitting remains a frontier research topic in the quest to develop artificial photosynthetic systems by using noble metal-free and sustainable catalysts. Herein, a highly crystalline CuSe has been employed as active electrodes for overall water splitting (OWS) in alkaline media. The pure-phase klockmannite CuSe deposited on highly conducting nickel foam (NF) electrodes by electrophoretic deposition (EPD) displayed an overpotential of merely 297 mV for the reaction of oxygen evolution (OER) at a current density of 10 mA cm^{-2} whereas an overpotential of 162 mV was attained for the hydrogen evolution reaction (HER) at the same current density, superseding the Cu-based as well as the state-of-the-art RuO$_2$ and IrO$_2$ catalysts. The bifunctional behavior of the catalyst has successfully been utilized to fabricate an overall water-splitting device, which exhibits a low cell voltage (1.68 V) with long-term stability. Post-catalytic analyses of the catalyst by ex-situ microscopic, spectroscopic, and analytical methods confirm that under both OER and HER conditions, the crystalline and conductive CuSe behaves as an electro(pre)catalyst forming a highly reactive in situ crystalline Cu(OH)$_2$ overlayer (electro(post)catalyst), which facilitates oxygen (O$_2$) evolution, and an amorphous Cu(OH)$_2$/CuO$_x$ active surface for hydrogen (H$_2$) evolution. The present study demonstrates a distinct approach to produce highly active copper-based catalysts starting from copper chalcogenides and could be used as a basis to enhance the performance in durable bifunctional overall water splitting.

Introduction

Rapid depletion of fossil fuels is driving the urgent requirement for alternative systems to harness energy.[1] Splitting of water into oxygen (O$_2$) and hydrogen (H$_2$) is one of the promising ways to overcome the current energy crisis, and this process is vital in natural photosynthesis, which directly converts photon energy to chemical energy.[2] In this regard, the development of artificial photosynthesis by mimicking nature's strategy has become an essential pathway for a clean and sustainable energy-based society.[3] However, the high thermodynamic barrier of the overall water splitting (OWS), which comprises two half-cell reactions—oxygen evolution reaction (OER) at the anode and hydrogen evolution reaction (HER) at the cathode—makes this process extremely demanding.[4] Therefore, the design of efficient bifunctional OER and HER catalysts to perform OWS remains a great challenge and deserves significant attention.[4,5] Currently, the state-of-the-art electrocatalysts to perform water splitting (WS) mainly rely on the noble-metal-based materials (RuO$_2$ and IrO$_2$ for OER, and Pt for HER).[6] However, the low abundance of these precious elements limits their wide practical application. Conversely, recent studies infer that higher OER or HER catalytic activity could be achieved by a subtle choice of Earth-abundant transition-metal (TM) based catalysts, particularly the first-row TMs.[7] However, only a few of them have been shown to mediate efficient bifunctionality for OWS.

On the other hand, copper is one of the most abundant metals and has immense biological significance.[8] Moreover, high catalytic activity and conductivity of metallic copper and/or copper-based materials have widely been used for organic transformations,[9] photothermal,[10] electrical and electronic devices.[11] Apart from this, copper and copper oxide nanomaterials have also been employed as efficient CO$_2$ reduction catalysts with profound catalytic efficacy.[9, 12] Most recently, in a handful cases, copper-based nanomaterials have also been applied as efficient electrocatalysts for OER.[13] In this direction,

[a] Dr. B. Chakraborty,+ R. Beltrán-Suito,+ Dr. P. W. Menezes, Prof. Dr. M. Driess
Department of Chemistry: Metalorganics and Inorganic Materials
Technische Universität Berlin
Straße des 17 Juni 135, Sekr. C2, 10623 Berlin (Germany)
E-mail: prashanth.menezes@mailbox.tu-berlin.de
matthias.driess@tu-berlin.de

[b] Dr. V. Hlukhyy
Department Chemie
Technische Universität München
Lichtenbergstraße 4, 85747 Garching (Germany)

[c] Dr. J. Schmidt
Department of Chemistry: Functional Materials
Technische Universität Berlin
Hardenbergstraße 40, 10623 Berlin (Germany)

[+] These authors contributed equally to this work.

ChemSusChem

Full Papers
doi.org/10.1002/cssc.202000445

Chemistry
Europe
European Chemical
Societies Publishing

copper pnictides and chalcogenides such as Cu_3N, Cu_3P, and Cu_9S_5 have gained considerable interest owing to their favorable OWS activity with low cell potential in alkaline electrolytes.[14] Under electrochemical conditions, both Cu_3N and Cu_3P nanostructures act as electro(pre)catalysts. They undergo an in situ transformation to form the electro(post)catalyst CuO_x overlayer, which efficiently accomplishes OER, HER, and OWS with remarkably low overpotential and cell potentials.[14a] In this context, copper chalcogenides are relatively less explored as OWS catalysts, and in the recent reports, Cu_2S and Cu_2Se have only been used as OER catalysts.[15] Consequently, the lack of activity for HER in copper chalcogenides prompted us to investigate a copper-based selenide (CuSe) as a potential bifunctional catalyst for OWS.[15a,b] Over the years, numerous TM selenides, mainly based on Fe, Co, and Ni have been uncovered as attractive bifunctional electrocatalysts in alkaline media.[7h,16] Although much is known about the electrical,[11d] electronic, and conducting[11a] properties of CuSe,[11b,c,17] its bifunctionality for OWS has never been documented.[5c]

Herein, we report, for the first time, a highly crystalline klockmannite CuSe as a bifunctional electro(pre)catalyst for the OWS reaction in alkaline electrolyte. CuSe has been synthesized from a high-temperature calcination approach, and without altering its chemical identity, the material has been deposited on highly conducting electrode substrates (nickel foam, NF, and fluorinated tin oxide, FTO) through the electrophoretic deposition (EPD) technique for simultaneous oxidation and reduction of water to O_2 and H_2, respectively. Impressively, the recorded overpotentials at a current density of $10\ mA\ cm^{-2}$ (297 mV for OER and 162 mV for HER) are among the best values reported for copper-based materials. When both anode and cathode are fabricated by using CuSe deposited on NF as electro(pre)catalyst for OWS, a low cell potential (1.68 V) with a faradaic efficiency of near 100% has been achieved. The detailed post-OER and HER analyses indicate the formation of a crystalline $Cu(OH)_2$ overlayer as an active phase for OER whereas an amorphous $Cu(OH)_2/CuO_x$ overlayer on the CuSe behaves as the active catalyst for the HER. Additionally, the conductive CuSe core accelerates the electron transport between the active layer and the electrode substrate. As Cu-based materials have a limited exposure for OER, HER, and OWS, the presented study opens a promising scope to explore new bifunctional catalytic systems based on copper.
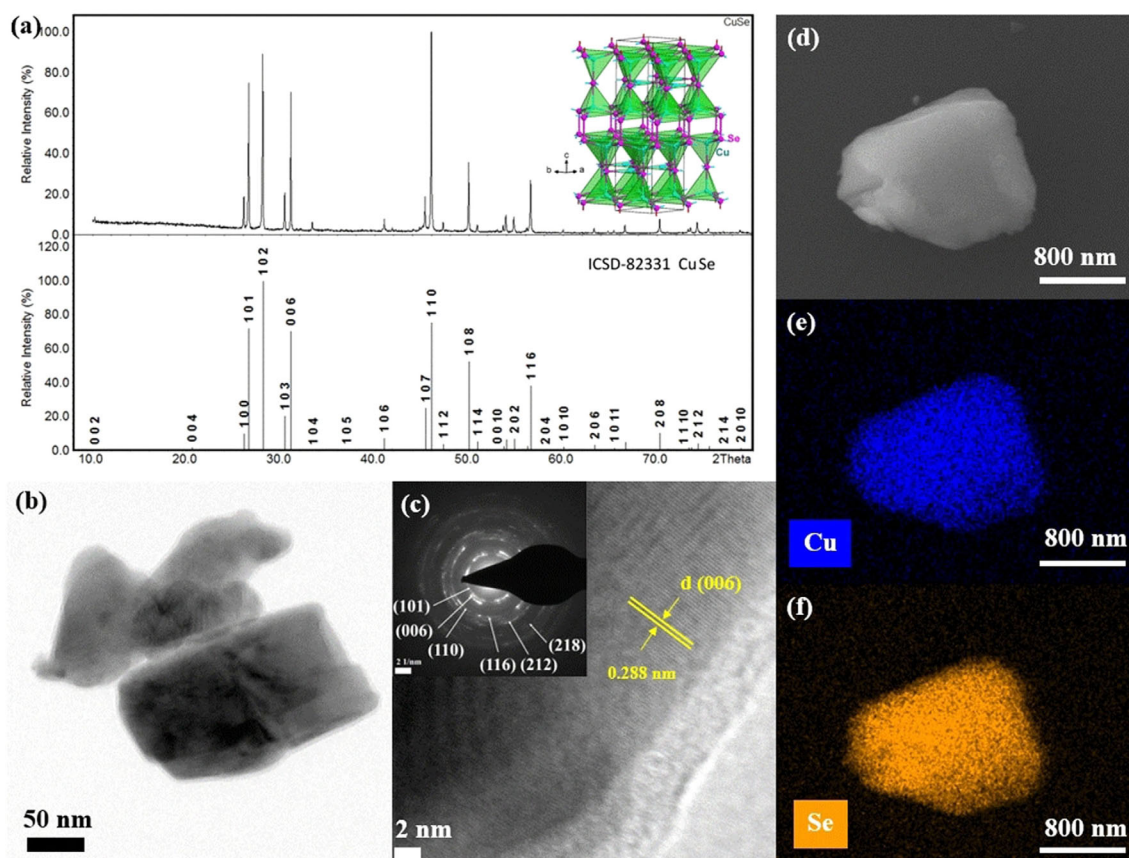
Results and Discussion

CuSe crystalline particles were synthesized by the high-temperature calcination of metallic copper and selenium powder in an inert atmosphere at a 900 °C (see the Experimental Section and the Supporting Information).[13] High crystallinity and phase purity of the as-prepared powder sample was confirmed by powder X-ray diffraction (XRD) analysis. The obtained diffraction patterns were consistent with the klockmannite CuSe (ICSD-82331; Figure 1a), and the crystal structure of the compound synthesized herein belongs to a hexagonal $P6_3/mmc$ group with lattice parameters $a = 3.9428(1)$ Å and $c = 17.2574(7)$ Å.[18] The arrangement of the Cu and Se atoms in

the unit cell results in a layered-type structure (Figure S1a in the Supporting Information) where each Cu^{II} ion is surrounded by four Se atoms possessing a tetrahedral geometry with a Cu–Se distance of 2.384–2.435 Å and Cu^I ion is trigonal-planar coordinated by Se atoms with Cu–Se distances of 2.276 Å. Two geometrically distinguishable (five- and four-coordinate) Se atoms present in the layered framework, and each four-coordinated Se atom is positioned in such a way that a Se–Se covalent type interaction occurs at a distance of 2.340 Å (Figure S1b in the Supporting Information).[18a]

Transmission electron microscopic (TEM) analysis of the as-prepared CuSe revealed large particles (ca. 200×120 nm; Figure 1b, Figure S2 in the Supporting Information). The high-resolution TEM image of a crystal provided lattice fringes matching with the $d(006)$ planes of CuSe with an inter-planar distance of 0.288 nm (Figure 1c). Selected area electron diffraction (SAED) analysis conducted on the particles displayed well-defined diffraction rings which could be correlated to the Miller indices $\{(101), (006), (110), (116), (212),$ and $(218)\}$ of CuSe (Figure 1c, inset). Scanning electron microscopic (SEM) images also illustrated the block morphology of the particles with varying sizes (Figure S3 in the Supporting Information). Elemental mapping of the particles confirmed the homogeneous distribution of Cu and Se (Figure 1d–f) whereas energy-dispersive X-ray (EDX) analysis showed a Cu/Se ratio of approximately 1:1 (Figures S4, S5, and Table S1 in the Supporting Information). An identical elemental composition was further confirmed by inductively coupled plasma atomic emission spectroscopy (ICP-AES) analysis of the powder sample (Table S1 in the Supporting Information).

To ascertain the elemental (oxidation) state of the CuSe material, X-ray photoelectron spectroscopic (XPS) studies were performed with the as-prepared powder. In the high-resolution XPS, the Cu 2p envelope consisted of two peaks corresponding to Cu $2p_{3/2}$ and Cu $2p_{1/2}$ at the binding energies of 932.1 eV and 952.2 eV, respectively (Figure S6a in the Supporting Information). The spin-orbit coupling spacing value ($2p_{3/2}$–$2p_{1/2}$) of 20.1 eV and the detailed deconvolution indicated the presence of Cu^I with an appreciable amount of Cu^{II} (Cu^I/Cu^{II} 1:0.11 ratio, Figure S6a in the Supporting Information). The Cu^I species belongs to the CuSe and Cu^{II} arises from the surface passivation owing to aerial oxidation. The presence of the latter species is consistent with earlier reports of $Cu_{2-x}Se$ and CuSe materials.[11c,18b,19] The Se 3d envelope recorded with the powder sample showed an overlapped spin-orbit component with two maxima for $3d_{5/2}$ and $3d_{3/2}$ peaks at 53.8 and 54.5 eV ($\Delta = 0.7$ eV). These energy values (after deconvolution) are consistent with the presence of Se^{II-}, as shown for reported CuSe materials.[11c,18b,19a] Moreover, a weak loss feature at 56.1 eV and a weak peak corresponding to Se^{IV} arising from surface passivation at 58.3 eV, as observed in other metal selenides (Figure S6b in the Supporting Information).[16c,20]

After an in-depth microscopic and spectroscopic analysis, the ground CuSe was deposited on NF (a three-dimensional and high surface area electrode substrate) through EPD. The as-deposited films of CuSe on NF were further analyzed by microscopic and analytical techniques, which confirmed the ex-

↖↖ These are not the final page numbers!

ChemSusChem

Full Papers
doi.org/10.1002/cssc.202000445

Chemistry Europe
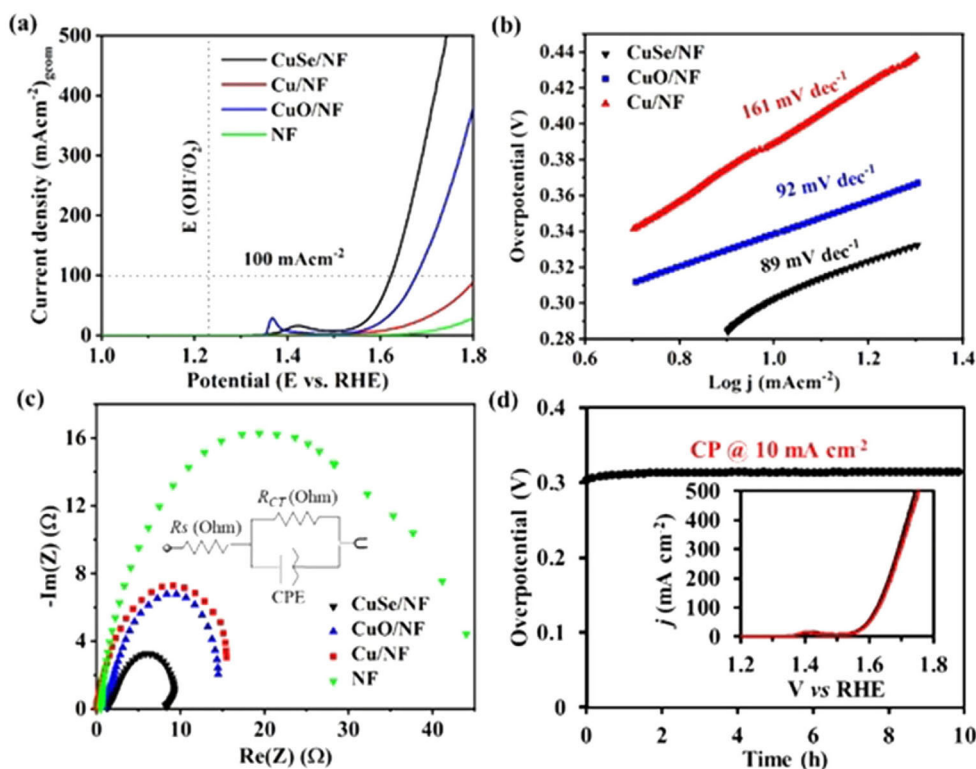European Chemical
Societies Publishing

Figure 1. Characterization of CuSe crystals. (a) Powder XRD pattern of the as-prepared CuSe, which consists of a sharp diffraction pattern matching CuSe ICSD-82331 (the crystal structure shown in the inset). (b) TEM images of the powder CuSe showing smaller crystals. (c) High-resolution TEM image with atomic fringes matches with the (006) lattice plane of CuSe, and SAED pattern exhibiting diffraction rings of CuSe (inset). (d) SEM image of CuSe particle with (e, f) EDX mapping, which displays a homogeneous distribution of elements Cu (blue) and Se (orange).

cellent chemical stability of CuSe after EPD (Figures S7–S9 in the Supporting Information). The electrocatalytic properties of CuSe were measured and compared with that of CuO and Cu nanoparticles. A three-electrode set-up in 1 M aqueous KOH electrolyte where catalysts deposited on NF served as the working electrode was used. The linear sweep voltammetry (LSV) curve displayed a slow increase in current density with the applied potential (Figure 2 a) and reached up to 500 mA cm^{-2} at 1.7 V (vs. reversible hydrogen electrode, RHE), indicating catalytic oxidation of water. The overpotentials recorded for the OER with CuSe/NF were 297 mV and 382 mV at 10 mA cm^{-2} and 100 mA cm^{-2}, respectively. A much lower current density resulted when CuO/NF and metallic Cu/NF were used as OER electrodes. The overpotential recorded with CuO/NF was 339 mV (at 10 mA cm^{-2}), whereas an overpotential of 389 mV (at 10 mA cm^{-2}) was achieved for Cu/NF. The bare NF measured in similar LSV conditions was almost inactive. Interestingly, the overpotential (297 mV) achieved with CuSe is slightly higher than the recently reported Cu$_2$Se (270 mV), which could arise from the stability of Cu$_2$Se under OER, the substrate effect (Cu substrate), different mass loading (5 mg), and the higher accessibility of Cu sites of Cu$_2$Se at the surface.[15b] The mass normalized activity and TOF of CuSe/NF, CuO/NF, and Cu/NF is summarized in Figures S10 and S11 (in the

Supporting Information), which further presented the superior activity of the CuSe/NF. Recent studies by the groups of Mayer, Brudvig, and Lin have highlighted that electrooxidation of water catalyzed by Cu^{II} complexes proceeds through an in situ formed active Cu^{III} intermediate and, in all the cases, a similar redox feature was observed.[21] By analogy to these studies, as well as other reported Cu-based heterogeneous catalysts, it could be proposed that under applied potentials, Cu^{III}O(OH) species were formed at the surface to catalyze the OER.[14a, 22]

To understand the electrokinetics of the OER, Tafel slopes were calculated from the Tafel plot (Figure 2 b). For CuSe/NF, a Tafel slope of 89 mV dec^{-1} was attained, which was significantly lower than CuO/NF (92 mV dec^{-1}) and Cu/NF (161 mV dec^{-1}), indicating faster OER kinetics of CuSe/NF. To evaluate the electron transfer capacity, electrochemical impedance spectra (EIS) were recorded. The semicircular Nyquist plot depicts a considerably low charge-transfer resistance (R_{ct}) for CuSe/NF (Table S2 in the Supporting Information) compared with those of other materials, suggesting a facile electron transfer between the substrate electrode surface and CuSe catalyst providing better OER activity (Figure 2 c).[23] The electrochemical double-layer capacitance (C_{dl}) was further determined by collecting CVs in a non-faradic region (Figure S12 in the Supporting Information) and, consequently, the electrochemically active surface area

These are not the final page numbers! ↗↗

ChemSusChem

Full Papers
doi.org/10.1002/cssc.202000445

Chemistry Europe
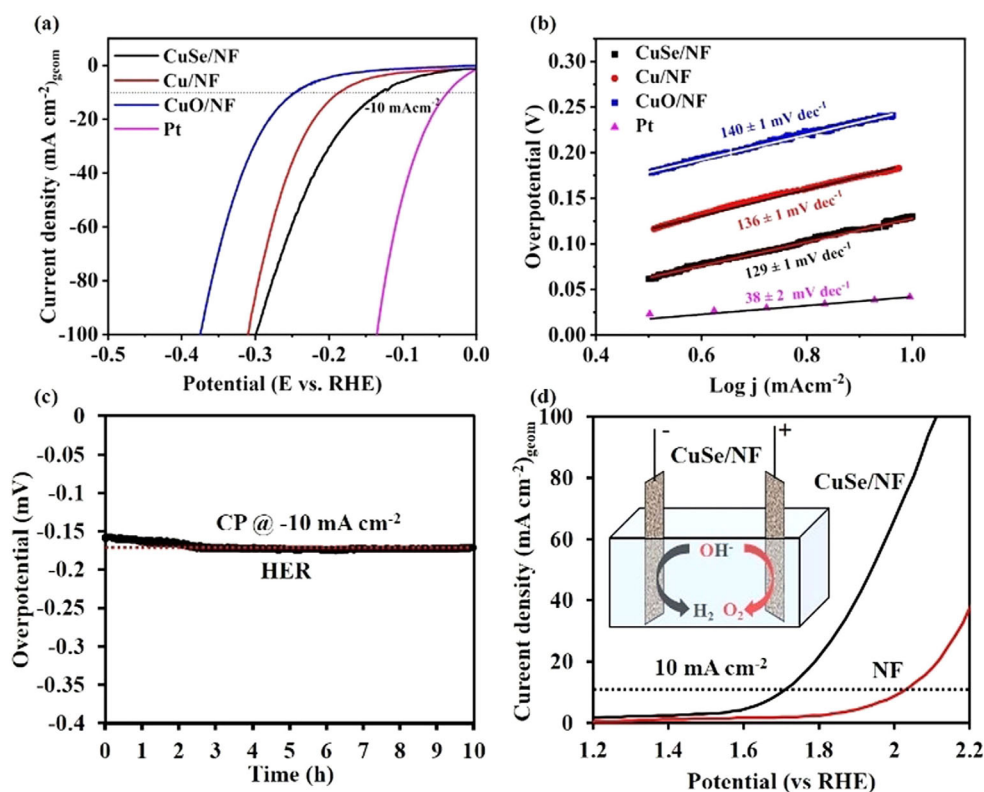European Chemical
Societies Publishing

Figure 2. Electrochemical study of CuSe, CuO, and Cu on NF. (a) Polarization curves from LSV for OER, (b) Tafel plot, (c) Nyquist plot from EIS analysis, and (d) the chronopotentiometry (CP) measurements at a current density of 10 mA cm^{-2} (OER) for 10 h. (d, inset) LSV measured before (black) and after 10 h of CP (OER) experiment (red), exhibiting almost overlapped polarization curves demonstrating the remarkable stability of CuSe. The LSV and Tafel slopes were recorded at a scan rate of 1 mV s^{-1}.

(ECSA), which is proportional to the C_{dl} was obtained.[7b] A C_{dl} of 1.45 mF cm^{-2}, calculated for CuSe/NF was higher than that of CuO/NF (1.0 mF cm^{-2}) and Cu/NF (0.98 mF cm^{-2}) as well as nine-fold larger compared with bare NF (0.16 mF cm^{-2}; Table S3 in the Supporting Information).[24] A higher value of the ECSA normalized current density further pointed out the better intrinsic activity (Figure S13 in the Supporting Information) of CuSe/NF within the investigated materials. To assess the long-term durability of CuSe/NF, a chronopotentiometry (CP) measurement was conducted, maintaining a current density of 10 mA cm^{-2}, which substantiated the inherent stability of the catalyst in the long run (Figure 2d). The sustainable activity of CuSe/NF was further demonstrated by measuring the LSV before and after OER CP catalysis (Figure 2d, inset). Furthermore, the performance of CuSe/NF was compared with the benchmark RuO$_2$/NF and IrO$_2$/NF catalysts (Figure S14 in the Supporting Information), and the resulting overpotential of CuSe/NF was strikingly better than that of noble-metal-based catalysts, making it one of the most proficient OER catalysts designed from earth-abundant first-row transition metals. In addition, the catalytic OER activity achieved here is not only superior to well established copper oxide and/or hydroxides but also comparable to Cu$_9$S$_5$, Cu$_3$N, Cu$_3$P, and Cu$_2$Se materials (Table S4 in the Supporting Information).[14a–c,e,f,15b] Moreover, the overpotential of CuSe/NF even surpasses some of the Co,

Fe, and Ni-containing active electrocatalysts reported in the literature.[7b, 25]

Recent reports have revealed that metallic copper and copper-based materials can act as potential reduction catalysts.[9, 12, 26] Additionally, the bifunctional behavior of the previously reported Fe,[7h] Co,[16c] and Ni[16b] selenide materials towards WS inspired us to study HER with CuSe/NF films. Subsequently, the CuSe/NF catalyst was tested as a working electrode for HER in 1 M aqueous KOH solution in a similar fashion as that of OER. A graphite rod, instead of Pt as the reference electrode was used to rule out the influence of Pt (leaching and redeposition on the working electrode). From the LSV polarization curves, an overpotential of 162 mV was achieved for CuSe/NF at a current density of −10 mA cm^{-2} (Figure 3a), whereas CuO/NF (245 mV) and Cu/NF (186 mV) recorded significantly high overpotentials at the same current density. Similar to OER, NF showed limited activity; however, Pt was the most active for HER among the tested catalysts. Notably, the overpotential of CuSe/NF is closely comparable to the recently reported copper and other transition metal-based HER catalysts (Table S5 in the Supporting Information).[27] The mass and ECSA normalized activity and TOF of CuSe/NF, CuO/NF, and Cu/NF are shown in Figures S15–S17 (in the Supporting Information). Further, a Tafel slope of 129 mV dec^{-1} resulted from CuSe/NF, which was lower than Cu/NF (136 mV dec^{-1}) and CuO/NF (140 mV dec^{-1}) displaying faster kinetics for HER catalysis (Fig-

↖↖ **These are not the final page numbers!**

ChemSusChem

Full Papers
doi.org/10.1002/cssc.202000445

Chemistry
Europe
European Chemical
Societies Publishing

Figure 3. Electrochemical HER and OWS with CuSe/NF. (a) Polarization curves of HER of CuSe/NF compared with Cu/NF, CuO/NF, Pt, and bare NF. (b) Tafel plot (along with Tafel slopes) obtained from the LSV curves for HER measurements with CuSe, Cu, CuO, and Pt. (c) HER CP of CuSe at a constant current of $-10\,mA\,cm^{-2}$ in a three-electrode set-up. (d) Polarization curve of OWS in the two-electrode set-up (c, inset) using CuSe/NF as both cathode and anode.

ure 3b). The CuSe/NF catalyst was tested under CP conditions at a constant current density $-10\,mA\,cm^{-2}$ for HER (Figure 3c), and a marginal drop in overpotentials was observed, highlighting its superior stability.
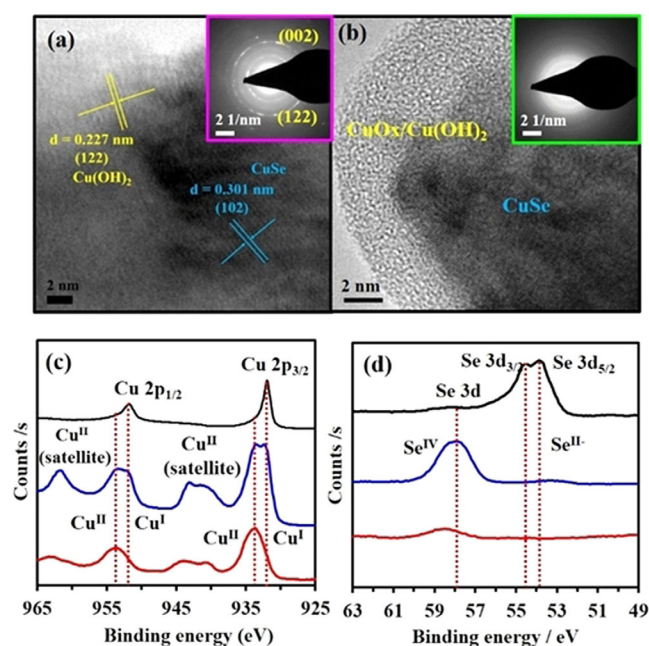
It has been documented previously that the electrode support plays a crucial role in electrocatalysis.[7f,g,28] To verify this, CuSe, CuO, and Cu were electrophoretically deposited on FTO, characterized (Figures S18–S21 in the Supporting Information), and then measured similarly to that of the NF substrate in 1 M aqueous KOH electrolyte (Figures S22–S23 in the Supporting Information). Under the tested OER conditions, the overpotential of CuSe/FTO was found to be 380 mV at a current density of 10 mA cm^{-2}, whereas CuO/FTO and Cu/FTO displayed an overpotential of 455 and 610 mV, respectively (Figure S22 in the Supporting Information). Similarly, CuSe/FTO also outperformed CuO/FTO and Cu/FTO in HER conditions (Figure S23 in the Supporting Information). Notably, the catalytic performance of CuSe for both OER and HER based on FTO followed the same trend as that of NF.

Inspired by the promising catalytic half-cell activities for OER and HER, we designed an OWS device with a two-electrode configuration by using CuSe/NF as both anode and cathode in 1 M aqueous KOH electrolyte at room temperature (Figure 3d, inset and Figure S24 in the Supporting Information). The polarization curve in Figure 3d shows the high performance of CuSe/NF, reaching a current density of 10 mA cm^{-2} with a requirement of cell voltage of 1.68 V whereas bare NF displayed

a large cell voltage (>2 V). Notably, the catalytic OWS performance of CuSe/NF is clearly higher than the recently reported monometallic selenides, better than mono and bimetallic chalcogenide materials, and comparable with other highly active non-noble based bifunctional electrocatalysts (Table S6 in the Supporting Information).[16,14f,15b] The long-term stability (CP) of this bifunctional catalyst was also tested in similar conditions at a current density of 10 mA cm^{-2}, which demonstrated the superior durability of the electrodes (Figure S25 in the Supporting Information). To demonstrate the efficiency of the catalysts, an inverted (graduated) electrolyzer cell was constructed and the relative evolution of H$_2$ to that of O$_2$ gas was collected separately at atmospheric pressure (Figure S26 in the Supporting Information). The measured volume of the evolved O$_2$ and H$_2$ at the anode and cathode followed the theoretically predicated 1:2 ratio (Figure S27 in the Supporting Information). In a separate experiment, under a closed electrochemical cell, the evolved gases were further quantified by GC analysis, and that gave almost 90% and 98% faradaic efficiency for OER and HER, respectively (Table S7 in the Supporting Information).

After obtaining successful results for each half-reaction of OER and HER, the structure of the active catalysts on the electrode was systematically investigated through various ex situ methods. Previous studies have confirmed that under alkaline electrochemical OER and HER operational conditions, the surface of non-oxide materials such as TM chalcogenides, phosphides, phosphates, as well as intermetallic compounds, under-

These are not the final page numbers! ↗↗

ChemSusChem

Full Papers
doi.org/10.1002/cssc.202000445

Chemistry
Europe
European Chemical
Societies Publishing

goes a rapid structural change forming a highly reactive metal oxide/hydroxide/oxyhydroxide.[7g,h,29] In this regard, we examined the CuSe electrodes separately after CP measurements (termed as OER CP and HER CP hereafter) by spectroscopic, microscopic, and analytical methods to gain detailed insights. The TEM measured after OER CP suggested a severe morphological and structural change compared with the as-prepared material. The high-resolution TEM images provided concrete evidence in support of the formation of crystalline $Cu(OH)_2$ (Figure 4a and Figure S28 in the Supporting Information) on the surface and were further evidenced by the well-defined diffraction rings of $Cu(OH)_2$ in the SAED pattern (Figure 4a, inset, JCPDS 42-746). The TEM also showed the remaining crystalline CuSe core identified by the lattice fringes matching with the $d(1\bar{0}2)$ planes with an inter-planar distance of 0.301 nm. The elemental analysis (SEM and EDX) of the catalyst after OER CP exhibited a significant loss of Se from the catalyst surface and concomitant oxygen incorporation into the structure (Figures S29–S30 in the Supporting Information). This is in accordance with the formation of a layer-type $Cu(OH)_2$.[30] The ratio of Cu and Se in the electrolyte solution was determined by ICP-AES analysis, which also supported the loss of Se ($\approx 40\%$; Table S8 in the Supporting Information). However, under HER CP, TEM and SAED analyses showed the formation of an amorphous overlayer on the crystalline CuSe, which was predicted to be an amorphous copper oxide/hydroxide (Figure 4b, Figure S31 in the Supporting Information). Elemental mapping

(SEM and EDX) confirmed the presence of oxygen in the amorphous layer structure (Figures S32–S33 in the Supporting Information). ICP-AES analysis of the electrolyte after HER indicated a similar extent of Se loss (Table S9 in the Supporting Information) in comparison to that observed for OER CP.

To analyze the change in the surface structure, XPS was conducted after OER CP and HER CP and compared directly with the deposited CuSe electrode. The binding energy values of Cu 2p and Se 3d, in addition to their spin-orbit coupling values ($2p_{1/2}$–$2p_{3/2}$), differ dramatically after CP for both OER and HER (Figure 4c–d). In the deconvoluted Cu 2p spectrum recorded after OER CP (Figure 4c, blue curve), two higher binding energy peaks (Cu $2p_{3/2}$ 933.3 eV and Cu $2p_{1/2}$ 953.7 eV) appeared with two major satellite peaks (at 944.8 and 961.7 eV) indicating a higher amount of Cu^{II} from $Cu(OH)_2$ on the surface in comparison to the as-prepared film, which is almost pure Cu^{I} (Figure 4c, Figure S34a in the Supporting Information). Despite the oxidation of Cu^{I} to Cu^{II} on the surface, peaks for Cu^{I} were still present (Cu $2p_{3/2}$ 932.8 eV and Cu $2p_{1/2}$ 952.2 eV), demonstrating that the CuSe core was preserved after OER (Figure S34a in the Supporting Information).[15b] However, in the high-resolution XPS of Se, two strongly overlapped Se $3d_{5/2}$ and $3d_{3/2}$ binding energies (Figure 4d, black curve, and Figure S34b in the Supporting Information) mostly disappeared after OER CP and a broad peak appeared at 57.8 eV confirming the presence of Se^{IV} from SeO_x, formed during the alkaline electrochemical condition by oxidation of Se (blue and red curves). Such oxidation of Cu and Se under OER in strongly alkaline conditions has already been well documented for copper selenides.[11c,16c,18b,19a,20] Interestingly, the O 1s spectrum after OER CP displayed a sharp peak at 531.2 eV, suggesting the formation of $Cu(OH)_2$ (Figure S34c in the Supporting Information), in accordance with TEM and SAED results. On the other hand, similar to OER CP, slightly oxidized Cu 2p and completely oxidized Se 3d spectra were obtained after HER CP (Figure 4c–d, red curves). However, the O 1s spectrum of HER CP showed two prominent peaks 529.2 and 531.3 eV, strongly supporting the formation of CuO_x and $Cu(OH)_2$ surface (Figure S35c in the Supporting Information). Moreover, this observation can also be linked to the amorphous surface structure as displayed by TEM images (Figure 4d and Figure S31 in the Supporting Information). Detailed comparison of the high-resolution XPS spectra for Cu 2p, Se 3d, and O 1s of OER and HER CP has been provided in the Supporting Information (Figures S34–S35). From the detailed investigation, it was clear that during OER, a crystalline $Cu(OH)_2$ overlayer behaves as the active catalyst whereas a mixed amorphous $Cu(OH)_2/CuO_x$ surface boosts the HER activity. Also, the conductive CuSe core in both cases accelerates the electron mobility between the active catalyst to the electrode substrate, illustrating the dual benefit of the CuSe for electrocatalysis.[7h,14a,25c,31]

The post-(electro)catalytic characterization of CuSe confirmed the formation of two different active phases under OER and HER conditions. Based on the obtained results, the higher catalytic activity of CuSe for OER can be attributed to the formation of the in situ crystalline $Cu(OH)_2$ overlayer, which could form Cu^{III} species to facilitate O–O bond formation.[14a,-

Figure 4. Post-catalytic characterization of CuSe catalysts. (a) The high-resolution TEM image of the catalysts after OER CP where the Bragg's planes match perfectly with $Cu(OH)_2$ and the remaining CuSe core. The SAED (inset a) shows the diffraction rings matching to (002) and (122) from $Cu(OH)_2$. (b) TEM image after HER CP displaying the formation of an amorphous CuO_x layer surrounding the crystalline CuSe core. The SAED (b, inset) confirms the formation of an amorphous layer. Plots of XPS analysis for (c) Cu 2p and (d) Se 3d scans of the catalysts before (black), after OER CP (blue) and after HER CP (red).

↖↖ **These are not the final page numbers!**

ChemSusChem

Full Papers
doi.org/10.1002/cssc.202000445

Chemistry Europe
European Chemical
Societies Publishing

[c,e, 22a,c, 31, 32] Alternatively, the amorphous $Cu(OH)_2/CuO_x$ overlayer possibly creates a low-valent Cu species to catalyze the reaction of HER, as known for other Cu-based materials.[13, 14c,d, 27a] Moreover, it has also been shown that selenides have optimum bond strength to adsorb protons and can act as a base to accelerate deprotonation to furnish H_2 evolution.[7d,h, 16a,b] As the core of the particle still contained CuSe, the possibility of having selenium on the surface cannot entirely be ruled out. Similarly, the loss of Se from the surface of CuSe in both OER and HER could provide abundant defects and disorders, which has often been shown to be beneficial for electrocatalysis.[7-g, 14a, 29b,c, 33] Most importantly, the conductive core of CuSe sandwiched between the surface layer and the electrode substrate, enhances the charge mobility for both OER and HER (as also shown by EIS).[5a, 7h, 14a] Finally, the large ECSA of CuSe furnishes the increased number of active sites, favoring the efficient adsorption and transfer of reactants to accelerate the electrochemical reaction.[7f,g, 25c, 28b, 33, 34]

Conclusions

CuSe crystalline particles have been synthesized by using a high-temperature solid-state synthetic approach. The CuSe nanostructure behaves as an effective electro(pre)catalyst in alkaline media, displaying considerably low overpotentials for both reactions of OER and HER. Under OER conditions, the as-prepared CuSe generates an in situ crystalline $Cu(OH)_2$ overlayer that acts as the active site to facilitate O—O bond formation, whereas in HER, an amorphous $Cu(OH)_2/CuO_x$ shell is formed, which generates low-valent Cu species (alongside Se) to efficiently adsorb protons to evolve H_2. The superior conductivity of CuSe present at the core also plays a vital role by enhancing the charge transport between the active layer and the electrode surface for both OER and HER. Additionally, the loss of Se creates surface defects by increasing the active surface area to boost the catalytic activity of CuSe precatalyst. Keeping the activity and conductivity of the presented catalyst in mind, we have examined CuO and Cu for OER and HER, which validates our reasons for the higher activity of CuSe. Finally, the bifunctionality of CuSe has also been demonstrated by fabricating a two-electrode alkaline electrolyzer for OWS, which only requires a cell voltage of 1.68 V to reach 10 mA cm^{-2}. In the quest to design a novel catalyst relying on noble-metal-free and earth-abundant sources, the present study opens up new opportunities to modulate the active and electronic structure of electrocatalysts for practical water electrolysis.

Experimental Section

General considerations and instrumentation

All synthetic procedures related to the preparation of CuSe were carried out under inert conditions by using standard Schlenk techniques or an MBraun inert atmosphere dry box containing an atmosphere of purified nitrogen. The commercial RuO_2 (99%), IrO_2 (99%), and copper(II) acetate monohydrate were purchased from Alfa Aesar. Nickel foam (NF) and fluorine-doped tin oxide (FTO, resistivity 8–12 Ω sq^{-1}) were obtained from Racemat BV and Sigma–

Aldrich, respectively. Microscopic and spectroscopic characterizations and details of electrochemical measurements are provided in the Supporting Information.

Synthesis of CuSe

For the synthesis of the CuSe, all materials were handled in an argon atmosphere by using an argon-filled glovebox (MBraun, H_2O/O_2 level < 1.0 ppm) and other standard inert gas techniques. A binary CuSe compound was prepared from elemental copper and selenium in a stoichiometric ratio: Cu wire (5.62 mmol, purity 99.9%, Chem Pur) and Se granules (5.62 mmol, purity 99.999%, Chem Pur) were filled in double-walled silica glass ampules and sealed by using a O_2/H_2 flame in argon atmosphere (0.6 atm). The ampule was heated in a muffle furnace (Nabertherm, P330 controller) to 500 °C at a rate of 3 K min^{-1}, held at this temperature for 4 h, then heated to 900 °C at a rate of 3 K min^{-1}, and held at this temperature for 5 h. In the next step, the sample was slowly cooled to 300 °C at a rate of 5 K min^{-1}, held at this temperature for 20 h, and finally cooled down to room temperature at a rate of 10 K min^{-1}. An air-stable crystalline dark product was obtained from the reaction. The powder XRD pattern of the product shows the presence of the CuSe phase (see Figure 1 a).

Synthesis of Cu and CuO

Copper(II) acetate monohydrate (300 mg) was heated to 300 °C while the temperature was increased slowly with a heating rate of 5 °C min^{-1} and in the presence of a H_2 flow (slow, 2–3 L h^{-1}) and the temperature was maintained for 2 h. The resulting black powder sample was thoroughly washed with water and ethanol (3×50 mL) and dried at 60 °C to obtain 100 mg (yield >90%) of phase pure Cu. Following a very similar procedure, CuO (yield >95%) nanoparticles (NP) were obtained whereas the heating was done in presence of O_2 flow.

Conflict of interest

The authors declare no conflict of interest.

Keywords: copper selenide · electrocatalysis · klockmannite · non-noble metal catalyst · overall water splitting

[1] a) M. S. Dresselhaus, I. L. Thomas, *Nature* **2001**, *414*, 332–337; b) J. Qi, W. Zhang, R. Cao, *Adv. Energy Mater.* **2018**, *8*, 1701620; c) M. Höök, X. Tang, *Energy Policy* **2013**, *52*, 797–809.

[2] a) H. B. Gray, *Nat. Chem.* **2009**, *1*, 7; b) N.-T. Suen, S.-F. Hung, Q. Quan, N. Zhang, Y.-J. Xu, H. M. Chen, *Chem. Soc. Rev.* **2017**, *46*, 337–365; c) F. Song, L. Bai, A. Moysiadou, S. Lee, C. Hu, L. Liardet, X. Hu, *J. Am. Chem. Soc.* **2018**, *140*, 7748–7759; d) J. Li, R. Güttinger, R. Moré, F. Song, W. Wan, G. R. Patzke, *Chem. Soc. Rev.* **2017**, *46*, 6124–6147.

ChemSusChem

Full Papers
doi.org/10.1002/cssc.202000445

Chemistry
Europe
European Chemical
Societies Publishing

[3] a) T. A. Faunce, W. Lubitz, A. W. Rutherford, D. MacFarlane, G. F. Moore, P. Yang, D. G. Nocera, T. A. Moore, D. H. Gregory, S. Fukuzumi, K. B. Yoon, F. A. Armstrong, M. R. Wasielewski, S. Styring, *Energy Environ. Sci.* **2013**, *6*, 695–698; b) P. W. Menezes, A. Indra, F. Schuster, M. Schwarze, M. Driess, *ChemPlusChem* **2016**, *81*, 1068–1074; c) C. Bozal-Ginesta, J. R. Durrant, *Faraday Discuss.* **2019**, *215*, 439–451; d) J. J. Concepcion, R. L. House, J. M. Papanikolas, T. J. Meyer, *Proc. Natl. Acad. Sci. USA* **2012**, *109*, 15560–15564; e) X. Long, W. Qiu, Z. Wang, Y. Wang, S. Yang, *Mater. Today Chem.* **2019**, *11*, 16–28.

[4] B. You, Y. Sun, *Acc. Chem. Res.* **2018**, *51*, 1571–1580.

[5] a) C. Panda, P. W. Menezes, M. Driess, *Angew. Chem. Int. Ed.* **2018**, *57*, 11130–11139; *Angew. Chem.* **2018**, *130*, 11298–11308; b) B. Chakraborty, G. Gan-Or, Y. Duan, M. Raula, I. A. Weinstock, *Angew. Chem. Int. Ed.* **2019**, *58*, 6584–6589; *Angew. Chem.* **2019**, *131*, 6656–6661; c) B. Chakraborty, G. Gan-Or, M. Raula, E. Gadot, I. A. Weinstock, *Nat. Commun.* **2018**, *9*, 4896.

[6] a) T. Reier, M. Oezaslan, P. Strasser, *ACS Catal.* **2012**, *2*, 1765–1772; b) Y. Jiao, Y. Zheng, M. Jaroniec, S. Z. Qiao, *Chem. Soc. Rev.* **2015**, *44*, 2060–2086.

[7] a) I. Roger, M. A. Shipman, M. D. Symes, *Nat. Rev. Chem.* **2017**, *1*, 928; b) C. C. L. McCrory, S. Jung, J. C. Peters, T. F. Jaramillo, *J. Am. Chem. Soc.* **2013**, *135*, 16977–16987; c) B. M. Hunter, H. B. Gray, A. M. Müller, *Chem. Rev.* **2016**, *116*, 14120–14136; d) S. Anantharaj, S. R. Ede, K. Sakthikumar, K. Karthick, S. Mishra, S. Kundu, *ACS Catal.* **2016**, *6*, 8069–8097; e) K. N. Dinh, Q. Liang, C.-F. Du, J. Zhao, A. I. Y. Tok, H. Mao, Q. Yan, *Nano Today* **2019**, *25*, 99–121; f) P. W. Menezes, A. Indra, I. Zaharieva, C. Walter, S. Loos, S. Hoffmann, R. Schlögl, H. Dau, M. Driess, *Energy Environ. Sci.* **2019**, *12*, 988–999; g) P. W. Menezes, C. Panda, S. Loos, F. Bunschei-Bruns, C. Walter, M. Schwarze, X. Deng, H. Dau, M. Driess, *Energy Environ. Sci.* **2018**, *11*, 1287–1298; h) C. Panda, P. W. Menezes, C. Walter, S. Yao, M. E. Miehlich, V. Gutkin, K. Meyer, M. Driess, *Angew. Chem. Int. Ed.* **2017**, *56*, 10506–10510; *Angew. Chem.* **2017**, *129*, 10642–10646; i) F. Yu, L. Yu, I. K. Mishra, Y. Yu, Z. F. Ren, H. Q. Zhou, *Mater. Today Phys.* **2018**, *7*, 121–138; j) B. Chakraborty, A. Indra, P. V. Menezes, M. Driess, P. W. Menezes, *Mater. Today Chem.* **2020**, *15*, 100226.

[8] E. I. Solomon, D. E. Heppner, E. M. Johnston, J. W. Ginsbach, J. Cirera, M. Qayyum, M. T. Kieber-Emmons, C. H. Kjaergaard, R. G. Hadt, L. Tian, *Chem. Rev.* **2014**, *114*, 3659–3853.

[9] M. B. Gawande, A. Goswami, F.-X. Felpin, T. Asefa, X. Huang, R. Silva, X. Zou, R. Zboril, R. S. Varma, *Chem. Rev.* **2016**, *116*, 3722–3811.

[10] a) K. Shen, C. Hua, Z. Liang, Y. Wang, H. Sun, J. Hu, H. Zhang, H. Li, Z. Jiang, H. Huang, P. Wang, Z. Sun, E. Wahlström, Y. Lu, F. Song, *ACS Appl. Electron. Mater.* **2019**, *1*, 1817–1824; b) S. C. Singh, H. Li, C. Yao, Z. Zhan, W. Yu, Z. Yu, C. Guo, *Nano Energy* **2018**, *51*, 774–785.

[11] a) P. Pazhamalai, K. Krishnamoorthy, S. J. Kim, *Int. J. Hydrogen Energy* **2016**, *41*, 14830–14835; b) J. Gong, J.-C. Li, J. Yang, S. Zhao, Z. Yang, K. Zhang, J. Bao, H. Pang, M. Han, *ACS Appl. Mater. Interfaces* **2018**, *10*, 38341–38349; c) J. Choi, N. Kang, H. Y. Yang, H. J. Kim, S. U. Son, *Chem. Mater.* **2010**, *22*, 3586–3588; d) Y.-Q. Liu, F.-X. Wang, Y. Xiao, H.-D. Peng, H.-J. Zhong, Z.-H. Liu, G.-B. Pan, *Sci. Rep.* **2014**, *4*, 5998.

[12] C. W. Li, M. W. Kanan, *J. Am. Chem. Soc.* **2012**, *134*, 7231–7234.

[13] X. Liu, H. Zheng, Z. Sun, A. Han, P. Du, *ACS Catal.* **2015**, *5*, 1530–1538.

[14] a) C. Panda, P. W. Menezes, M. Zheng, S. Orthmann, M. Driess, *ACS Energy Lett.* **2019**, *4*, 747–754; b) A. Han, H. Zhang, R. Yuan, H. Ji, P. Du, *ACS Appl. Mater. Interfaces* **2017**, *9*, 2240–2248; c) J. Tian, Q. Liu, N. Cheng, A. M. Asiri, X. Sun, *Angew. Chem. Int. Ed.* **2014**, *53*, 9577–9581; *Angew. Chem.* **2014**, *126*, 9731–9735; d) J. Hao, W. Yang, Z. Huang, C. Zhang, *Adv. Mater. Interfaces* **2016**, *3*, 1600236; e) J. Du, F. Li, Y. Wang, Y. Zhu, L. Sun, *ChemElectroChem* **2018**, *5*, 2064–2068; f) B. Chakraborty, S. Kalra, R. Beltrán-Suito, C. Das, T. Hellmann, P. W. Menezes, M. Driess, *Chem. Asian J.* **2020**, 15, 852–859.

[15] a) Q. Li, X. Wang, K. Tang, M. Wang, C. Wang, C. Yan, *ACS Nano* **2017**, *11*, 12230–12239; b) J. Masud, W. P. R. Liyanage, X. Cao, A. Saxena, M. Nath, *ACS Appl. Energy Mater.* **2018**, *1*, 4075–4083; c) X. Zhao, L. Liu, Y. Zhang, H. Zhang, Y. Wang, *Nanotechnology* **2017**, *28*, 345402.

[16] a) C. Tang, N. Cheng, Z. Pu, W. Xing, X. Sun, *Angew. Chem. Int. Ed.* **2015**, *54*, 9351–9355; *Angew. Chem.* **2015**, *127*, 9483–9487; b) A. T. Swesi, J. Masud, W. P. R. Liyanage, S. Umapathi, E. Bohannan, J. Medvedeva, M.

Nath, *Sci. Rep.* **2017**, *7*, 2401; c) J. Masud, A. T. Swesi, W. P. R. Liyanage, M. Nath, *ACS Appl. Mater. Interfaces* **2016**, *8*, 17292–17302.

[17] R. Zhou, Y. Huang, J. Zhou, H. Niu, L. Wan, Y. Li, J. Xu, J. Xu, *Dalton Trans.* **2018**, *47*, 16587–16595.

[18] a) V. Milman, *Acta Crystallogr. Sect. B* **2002**, *58*, 437–447; b) Y. Xie, X. Zheng, X. Jiang, J. Lu, L. Zhu, *Inorg. Chem.* **2002**, *41*, 387–392.

[19] a) Y. Xie, A. Riedinger, M. Prato, A. Casu, A. Genovese, P. Guardia, S. Sottini, C. Sangregorio, K. Miszta, S. Ghosh, T. Pellegrino, L. Manna, *J. Am. Chem. Soc.* **2013**, *135*, 17630–17637; b) S. C. Singh, Y. Peng, J. Rutledge, C. Guo, *ACS Appl. Electron. Mater.* **2019**, *1*, 1169–1178.

[20] C. Wei, D. Zhong, D. Li, G. Hao, G. Liu, J. Li, Q. Zhao, *Int. J. Hydrogen Energy* **2019**, *44*, 21979–31986.

[21] a) K. J. Fisher, K. L. Materna, B. Q. Mercado, R. H. Crabtree, G. W. Brudvig, *ACS Catal.* **2017**, *7*, 3384–3387; b) T. Zhang, C. Wang, S. Liu, J.-L. Wang, W. Lin, *J. Am. Chem. Soc.* **2014**, *136*, 273–281; c) S. M. Barnett, K. I. Goldberg, J. M. Mayer, *Nat. Chem.* **2012**, *4*, 498–502.

[22] a) Y. Deng, A. D. Handoko, Y. Du, S. Xi, B. S. Yeo, *ACS Catal.* **2016**, *6*, 2473–2481; b) X. Liu, S. Cui, M. Qian, Z. Sun, P. Du, *Chem. Commun.* **2016**, *52*, 5546–5549; c) S. Cui, X. Liu, Z. Sun, P. Du, *ACS Sustainable Chem. Eng.* **2016**, *4*, 2593–2600.

[23] Q. Kang, L. Vernisse, R. C. Remsing, A. C. Thenuwara, S. L. Shumlas, I. G. McKendry, M. L. Klein, E. Borguet, M. J. Zdilla, D. R. Strongin, *J. Am. Chem. Soc.* **2017**, *139*, 1863–1870.

[24] Y. Yoon, B. Yan, Y. Surendranath, *J. Am. Chem. Soc.* **2018**, *140*, 2397–2400.

[25] a) Y. Rao, Y. Wang, H. Ning, P. Li, M. Wu, *ACS Appl. Mater. Interfaces* **2016**, *8*, 33601–33607; b) X. Zhang, H. Xu, X. Li, Y. Li, T. Yang, Y. Liang, *ACS Catal.* **2016**, *6*, 580–588; c) R. Beltrán-Suito, P. W. Menezes, M. Driess, *J. Mater. Chem. A* **2019**, *7*, 15749–15756.

[26] C. Ray, S. C. Lee, B. Jin, K. Y. Chung, S. Guo, S. Zhang, K. Zhang, J. H. Park, S. C. Jun, *ChemElectroChem* **2019**, *6*, 5014–5021.

[27] a) S. Wei, K. Qi, Z. Jin, J. Cao, W. Zheng, H. Chen, X. Cui, *ACS Omega* **2016**, *1*, 1367–1373; b) E. M. Nichols, J. J. Gallagher, C. Liu, Y. Su, J. Resasco, Y. Yu, Y. Sun, P. Yang, M. C. Y. Chang, C. J. Chang, *Proc. Natl. Acad. Sci. USA* **2015**, *112*, 11461–11466; c) Y. Sun, C. Liu, D. C. Grauer, J. Yano, J. R. Long, P. Yang, C. J. Chang, *J. Am. Chem. Soc.* **2013**, *135*, 17699–17702; d) C. Y. Son, I. H. Kwak, Y. R. Lim, J. Park, *Chem. Commun.* **2016**, *52*, 2819–2822.

[28] a) P. W. Menezes, A. Indra, C. Das, C. Walter, C. Göbel, V. Gutkin, D. Schmeißer, M. Driess, *ACS Catal.* **2017**, *7*, 103–109; b) C. Walter, P. W. Menezes, S. Orthmann, J. Schuch, P. Connor, B. Kaiser, M. Lerch, M. Driess, *Angew. Chem. Int. Ed.* **2018**, *57*, 698–702; *Angew. Chem.* **2018**, *130*, 706–710.

[29] a) A. Indra, P. W. Menezes, C. Das, C. Göbel, M. Tallarida, D. Schmeißer, M. Driess, *J. Mater. Chem. A* **2017**, *5*, 5171–5177; b) P. W. Menezes, C. Panda, S. Garai, C. Walter, A. Guiet, M. Driess, *Angew. Chem. Int. Ed.* **2018**, *57*, 15237–15242; *Angew. Chem.* **2018**, *130*, 15457–15462; c) P. W. Menezes, C. Walter, J. N. Hausmann, R. Beltran-Suito, C. Schlesiger, S. Praetz, V. Y. Verchenko, A. Shevelkov, M. Driess, *Angew. Chem. Int. Ed.* **2019**, *58*, 16569–16574; *Angew. Chem.* **2019**, *131*, 16722–16727.

[30] H. R. Oswald, A. Reller, H. W. Schmalle, E. Dubler, *Acta Crystallogr. Sect. C* **1990**, *46*, 2279–2284.

[31] P. W. Menezes, A. Indra, P. Littlewood, M. Schwarze, C. Göbel, R. Schomäcker, M. Driess, *ChemSusChem* **2014**, *7*, 2202–2211.

[32] a) J. Du, Z. Chen, S. Ye, B. J. Wiley, T. J. Meyer, *Angew. Chem. Int. Ed.* **2015**, *54*, 2073–2078; *Angew. Chem.* **2015**, *127*, 2101–2106; b) C.-C. Hou, W.-F. Fu, Y. Chen, *ChemSusChem* **2016**, *9*, 2069–2073.

[33] P. W. Menezes, C. Panda, C. Walter, M. Schwarze, M. Driess, *Adv. Funct. Mater.* **2019**, *29*, 1808632.

[34] C. Panda, P. W. Menezes, S. Yao, J. Schmidt, C. Walter, J. N. Hausmann, M. Driess, *J. Am. Chem. Soc.* **2019**, *141*, 13306–13310.

↖↖ **These are not the final page numbers!**

FULL PAPERS

Transform to perform: A highly crystalline klockmannite CuSe has been used as an efficient bifunctional electro(pre)catalyst for the reaction of alkaline water splitting and, subsequently, its active structure at the anode and cathode has been uncovered.

B. Chakraborty, R. Beltrán-Suito,
V. Hlukhyy, J. Schmidt, P. W. Menezes,*
M. Driess*

■■ – ■■

**Crystalline Copper Selenide as a
Reliable Non-Noble
Electro(pre)catalyst for Overall Water
Splitting**

These are not the final page numbers! ↗↗